CHEMMEDCHEM

DOI: 10.1002/cmdc.200800396

Structure–Activity Relationships and Binding Mode in the Human Acetylcholinesterase Active Site of Pseudo-Irreversible Inhibitors Related to Xanthostigmine

Stefano Rizzo,[a] Andrea Cavalli,*[a, b] Luisa Ceccarini,[a] Manuela Bartolini,[a] Federica Belluti,[a] Alessandra Bisi,[a] Vincenza Andrisano,[a] Maurizio Recanatini,[a] and Angela Rampa*[a]

Structure–activity relationship studies on acetylcholinesterase (AChE) inhibitors were extended to newly synthesized compounds derived from the lead compound xantostigmine (**1**). The xanthone ring of compound **1** was replaced with several different scaffolds based on the benzopyran skeleton, linked to the tertiary amino nitrogen through an heptyloxy chain. These modifications resulted in 19 new compounds, most of them showing activity in the nanomolar–subnanomolar range. Docking and molecular dynamics simulations were carried out to both define a new computational protocol for the simulation of pseudo-irreversibile AChE covalent inhibitors, and to acquire a better understanding of the structure–activity relationships of the present series of compounds. The results of this computational work prompted us to to evaluate the ability of compounds **5** and **13** to inhibit acetylcholinesterase-induced Aβ aggregation.

Introduction

Alzheimer's disease (AD), first described by Alois Alzheimer in 1907,[1] has become the most common cause of dementia in the elderly, affecting ~3% of the population between the age of 65 to 74, and nearly 50% of those 85 years and older.[2] The course of the devastating disease is marked by a progressive loss of brain functions such as memory and language skills, and life expectancy after diagnosis is ~8–10 years.

AD pathology is characterized by the production of extracellular senile plaques, mostly composed of aggregated β-amyloid peptide (Aβ),[3] in different areas of the brain, and intracellular neurofibrillary tangles, containing hyperphosphorylated Tau protein.[4]

During the past decade, treatment of patients with AD has been largely based on a strategy of enhancing acetylcholine (ACh)-mediated transmission. Symptomatic cognitive, functional and behavioral benefits[5,6] have been observed in multiple clinical trials with agents known to inhibit acetylcholinesterase (AChE) and butyrylcholinesterase (BuChE), both of which catalyze the breakdown of ACh. There is no doubt that significant dysfunction of the basal forebrain ACh system occurs in advanced AD, and therefore the development of cholinesterase (ChE) inhibitors was based on the well-accepted cholinergic hypothesis.[7] As a result, various ChE inhibitors, such as tacrine, donepezil, rivastigmine and galanthamine, have been launched onto the market.

Our research involves the development of AChE inhibitors as potential drugs for AD. Previously, we designed and studied a class of inhibitors (*N*-methyl-*N*-(3-carbamoyloxyphenyl)methylamino) characterized by the presence of a heteroaryl moiety linked to the tertiary amino nitrogen through an alkoxy chain. Xanthostigmine (**1**), the lead compound, showed the highest activity (IC_{50} = 0.3 nM).[8,9] A three-dimensional model of the quaternary complex between AChE and compound **1** showed

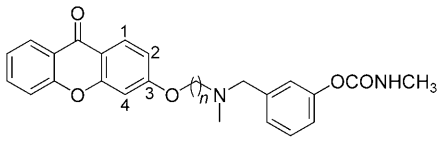

xanthostigmine (**1**), *n*=3
compound **2**, *n*=7

that the carbamate moiety is located in the active site of the enzyme for interaction with the catalytic triad, while the xanthone moiety points toward the opening of the gorge, caged within a framework of aromatic residues, but not within reach of the Trp279 residue (Torpedo californica AChE numbering), located at the entrance of the gorge. This aromatic residue, together with others, is considered to constitute an essential part of the AChE peripheral anionic site (PAS),[10–12] and recent studies have shown that inhibitors binding to this site are able to block the Aβ aggregation induced by AChE.[13–15]

In previous papers, we introduced modifications in the linker chain, the carbamoyl substituent and the aryl moiety of compound **1** in order to investigate the structure–activity relation-

[a] *S. Rizzo, A. Cavalli, L. Ceccarini, M. Bartolini, F. Belluti, A. Bisi, V. Andrisano, M. Recanatini, A. Rampa*
Department of Pharmaceutical Sciences, University of Bologna
Via Belmeloro 6, 40126 Bologna (Italy)
Fax: (+39) 051-2099734
E-mail: angela.rampa@unibo.it

[b] *A. Cavalli*
Unit of Drug Discovery and Development, Italian Institute of Technology
Via Morego 30, 16163 Genova (Italy)
Fax: (+39) 051-2099734
E-mail: andrea.cavalli@unibo.it

Supporting information for this article is available on the WWW under http://dx.doi.org/10.1002/cmdc.200800396.

ships (SAR) of this series of compounds.[16,17] A set of derivatives was rationally designed by properly lengthening the alkoxy chain linking the heterocyclic moiety to the tertiary amino group, in order to allow the heterocyclic system to establish π–π stacking interaction with the indole ring of Trp 279. Compound **2**, the seven methylene chain analogue of xanthostigmine,[16] being the most potent derivative of this series—equipotent but somewhat less selective than compound **1**—is able to simultaneously contact both the central anionic site (Trp 84) and the PAS.

The aim of this work was to further investigate the interactions of xanthostigmine analogues with the most important residues in the human acetylcholinesterase (hAChE) binding gorge, introducing one or two methoxy groups in positions 6 and 7 of the xanthone nucleus of compound **2** (compounds **3** and **4**), since these substituents could improve interaction with the PAS, as seen for both inhibitors donepezil[18] and AP2238.[19] In previous work, we studied the SAR of the heteroaryl moiety of compounds **1** and **2** by replacing the xanthone ring with several different systems based on the benzopyran skeleton, including coumarin and flavone derivatives, linked to the tertiary amino nitrogen through an alkoxy chain in position 7.[9] Herein, we focused our attention on phenylcoumarin (compounds **5**–**12**) and flavone (compounds **13**–**20**) derivatives and modified the position of the heptyloxy chain linking the tertiary amino nitrogen, which was placed on the phenyl ring in positions 3 and 2, respectively, in order to assess the influence of a different positioning of the polar heterocyclic nucleus. In particular, the chain was placed in *meta* and *para* positions on the phenyl ring to find the optimal orientation. Furthermore, one or two methoxy groups were introduced in positions 6 and 7 of the heterocycles in order to improve the interaction with the PAS. Finally, we introduced a methyl group in position 3 of the flavone core (compound **20**) to evaluate the effect of increased steric hindrance on activity.

To investigate the binding mode of the present series of derivatives and to more in depth describe the SAR data, computational studies were carried out using the crystallographic structure of the human isoform of the enzyme (PDB code 1B41). In particular, docking experiments were performed to identify a possible noncovalent binding interaction between the enzyme and inhibitors. Then, the quaternary complex was built between Ser 203 and the carbamate moiety of the compounds. Finally, molecular dynamics (MD) simulations were carried out in explicit solvent environments to investigate the dynamical behavior of the molecules in the enzyme binding site. These computations allowed us to better understand the SAR data of the inhibitors.

Results and Discussion

Chemistry

The synthesis of compounds **3**–**20** was accomplished as shown in Scheme 1. The synthesis of 3-hydroxyxanthones was reported in a previous paper.[20] The syntheses of hydroxycoumarins and hydroxyflavones are reported in the supporting information (schemes S1 and S2). The selected hydroxy derivatives were treated with 1,7-dibromoheptane in the presence of K_2CO_3 to afford the bromoheptyloxy derivatives **21 a-r**. These compounds were then condensed with *N*-(3-*h*ydroxybenzyl)-methylamine[9] to afford compounds **22 a-r**, which were treated with methyl isocyanate to give the desired compounds **3**–**20**. Full experimental details are given in the Experimental Section and Supporting Information.

Enzyme inhibition

The inhibitory activity of compounds **3**–**20** against AChE was studied using a method described by Ellman[21] to determine the rate of hydrolysis of acetylthiocholine in the presence of inhibitor. The selectivity of the compounds was also tested by determining their inhibitory activity against human BuChE.

Previously reported results showed that the carbamate analogues demonstrate a time-dependent pattern of inhibition.[9,16] In particular, the inhibition of both AChE and BuChE by carbamates involves a reversible complex formation, followed by carbamoylation of the enzyme to form a covalent adduct. The time required to reach the maximum inhibition for a given concentration of inhibitor dependents strongly on the steric bulk of the *N*-carbamic substituent. Therefore, to correctly evaluate the inhibitory potency, incubation times should be equal or longer than the time required for the formation of the covalent adduct.

Here, we did not determine the value of the carbamoylation constants for all of the compounds, but verified that even for

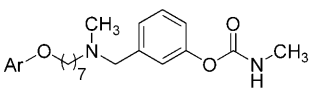

Ar= Z

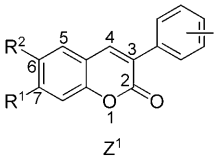

Z¹

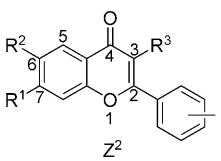

Z²

3, R^1=OCH_3, R^2=H
4, R^1=OCH_3, R^2=OCH_3

5, *para*, R^1=H, R^2=H
6, *para*, R^1=OCH_3, R^2=H
7, *para*, R^1=H, R^2=OCH_3
8, *para*, R^1=OCH_3, R^2=OCH_3
9, *meta*, R^1=H, R^2=H
10, *meta*, R^1=OCH_3, R^2=H
11, *meta*, R^1=H, R^2=OCH_3
12, *meta*, R^1=OCH_3, R^2=OCH_3

13, *para*, R^1=H, R^2=H, R^3=H
14, *para*, R^1=OCH_3, R^2=H, R^3=H
15, *para*, R^1=H, R^2=OCH_3, R^3=H
16, *meta*, R^1=H, R^2=H, R^3=H
17, *meta*, R^1=OCH_3, R^2=H, R^3=H
18, *meta*, R^1=H, R^2=OCH_3, R^3=H
19, *meta*, R^1=OCH_3, R^2=OCH_3, R^3=H
20, *para*, R^1=H, R^2=H, R^3=CH_3

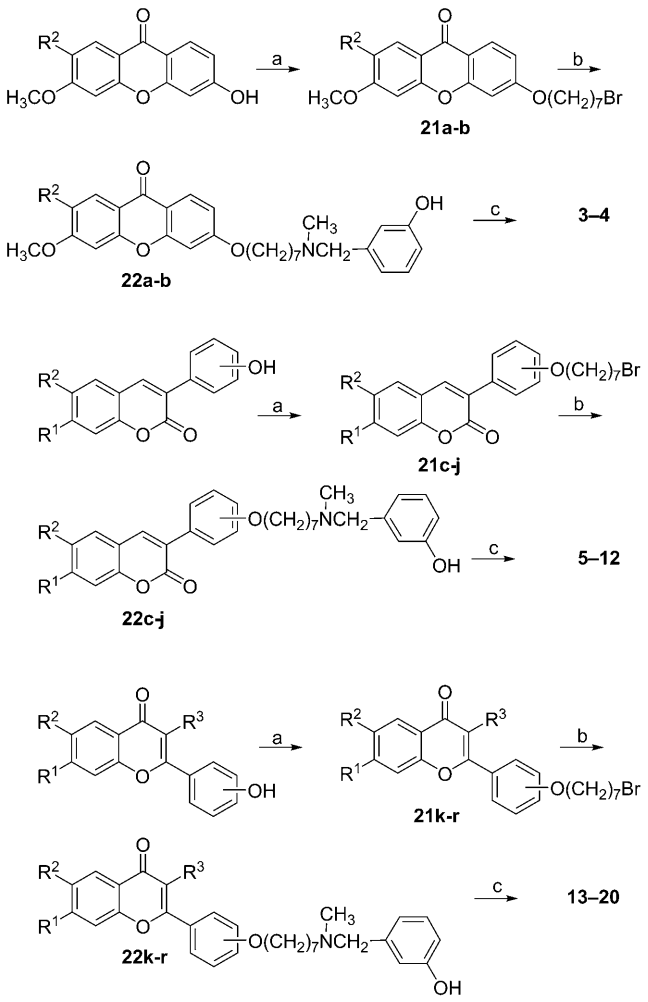

Scheme 1. Synthesis of inhibitors **3**–**20**. *Reagents and conditions*: a) Br-$(CH_2)_7$Br, K_2CO_3 reflux, 24 h; b) *N*-(3-hydroxybenzyl)methylamine, reflux, 15 h; c) CH_3NCO, NaH, RT, 24 h.

this series, the time required for the maximum inhibition fell within the incubation time (20 min) used for the Ellman's assay. Under these conditions, the IC_{50} values are indicative of the potency of inhibition and the risk of potency underestimation is overcome.

The inhibitory activities (IC_{50} values) of xanthostigmine derivatives against both hAChE and hBuChE, together with those of reference compounds **1** (xanthostigmine) and **2**, are reported in Table 1.

The aim of this work was to extend the SAR data of the ω-[*N*-methyl-*N*-(3-methylcarbamoyloxyphenyl)methyl]aminoheptyloxyaryl AChE inhibitors by varying specific structural features of the molecules. The results presented in Table 1 showed that the introduction of two methoxy groups (**4**) in reference compound **2** led to an order of magnitude decrease in activity, whereas the introduction of a methoxy group (**3**) in position 6 alone only slightly reduced activity, but improved selectivity toward AChE.

The xanthone moiety was substituted by a phenylcoumarin or flavone core bearing the alkoxyamine chain in the *meta* or *para* position on the phenyl ring. While all the coumarin derivatives (**5**–**12**) were less active than the parent compounds, the *para* substitution (**5**–**8**) was more favorable than the *meta* (**9**–**12**). Introduction of methoxy groups led to a further decrease in activity. Flavone derivatives (**13**–**20**) showed activity comparable to lead compound **2**. In this series, the substitution with the alkoxyamine chain on the phenyl ring led to a different effect compared to the coumarin derivatives. The *meta* position (**16**–**19**) proved to be more favorable than the *para* (**13**–**15**, **20**). Introduction of methoxy groups on the flavone had no influence on the AChE inhibitory activity of the *para* derivatives, but selectivity for AChE over BuChE was increased. Compounds **16** (no methoxy groups) and **17** (7-OCH_3) proved to be the most potent derivatives (0.52 and 0.51 nM, respectively), while a methoxy group in position 6 or disubstitution decreased the inhibitory activity. Selectivity was decreased for compounds carrying methoxy groups (**17**–**19**) with respect to the unsubstituted compound **16**. The increase in steric hindrance caused by the introduction of a methyl group in position 3 on the flavone core (compound **20**) was detrimental to the activity.

Docking, complex parameterization, and molecular dynamics simulations

Docking simulations were carried out using AutoDock 3.0.[22] Compounds **13** and **16** were docked in the binding gorge of hAChE (PDB code 1B41).[23] Docking simulations were aimed at identifying a possible binding mode resembling the Michaelis complex, which could then be modified to provide the covalent adduct. Indeed, AChE–carbamate-derived inhibitor co-crystal structures have suggested the formation of a quaternary covalent adduct as an intermediate.[24] A docking pose resembling the Michaelis complex was then exploited for the construction of the quaternary adduct, whose model system was optimized using density functional theory (DFT) computations at B3LYP/6-31G* level of theory, by keeping fixed the atoms of the protein backbone (see Supporting Information). New molecular mechanics parameters were derived, and four binary covalent complexes (AChE with compounds **13**, **16**, **5**, and **9**) were submitted to ns-time-scale molecular dynamics (MD) simulations performed with AMBER 8.0 (see Experimental Section for further details).[25]

Docking and MD simulations were carried out both to define a new computational protocol for the simulation of pseudo-irreversible AChE covalent inhibitors (see Experimental Section), and to rationalize the SAR results of the present series of compounds. Figure 1 reports the root mean square deviation (RMSD) against the simulation time for the four binary AChE–inhibitor complexes. Almost 5 ns of simulations were required to allow AChE–inhibitor complexes to stabilize. A conformation for each binary complex was extracted from stable simulation intervals, geometrically optimized, and analyzed to define a possible binding mode between the new inhibitor and AChE. The main interactions between AChE and compounds **5**, **9**, **13**, and **16** are described (Figure 2).

The AChE–**5** complex showed good stability during MD simulations (Figure 1 a). The negatively charged oxygen of the tet-

Table 1. Compounds **1**–**20** hAChE and hBuChE inhibition and selectivity data

Cmpd	Ar	R^1	R^2	R^3	chain position	hAChE[a] $IC_{50} \pm$ SEM (nM)	hBuChE[a] $IC_{50} \pm$ SEM (nM)	hBuChE/hAChE IC_{50} Ratio
1	Z	H	H	-	3	0.30 ± 0.01	48 ± 4	160
2	Z	H	H	-	3	0.32 ± 0.09	16.5 ± 1.4	52
3	Z	OCH_3	H	-	3	0.85 ± 0.18	76.2 ± 5.3	90
4	Z	OCH_3	OCH_3	-	3	1.56 ± 0.15	113 ± 9	72
5	Z^1	H	H	-	*para*	1.20 ± 0.09	59.4 ± 6.3	49
6	Z^1	OCH_3	H	-	*para*	5.99 ± 0.32	72.3 ± 2.5	12
7	Z^1	H	OCH_3	-	*para*	3.99 ± 0.26	38.3 ± 2.0	10
8	Z^1	OCH_3	OCH_3	-	*para*	10.9 ± 0.7	295 ± 17	27
9	Z^1	H	H	-	*meta*	3.59 ± 0.15	80.7 ± 9.4	22
10	Z^1	OCH_3	H	-	*meta*	2.72 ± 0.18	41.5 ± 4.8	15
11	Z^1	H	OCH_3	-	*meta*	6.58 ± 0.41	81.5 ± 5.0	12
12	Z^1	OCH_3	OCH_3	-	*meta*	3.16 ± 0.18	44.8 ± 3.6	14
13	Z^2	H	H	H	*para*	0.73 ± 0.05	70.2 ± 10.3	96
14	Z^2	OCH_3	H	H	*para*	0.72 ± 0.04	107 ± 7	149
15	Z^2	H	OCH_3	H	*para*	0.63 ± 0.02	91.0 ± 3.8	144
16	Z^2	H	H	H	*meta*	0.52 ± 0.03	63.7 ± 3.5	122
17	Z^2	OCH_3	H	H	*meta*	0.51 ± 0.06	57.4 ± 2.2	112
18	Z^2	H	OCH_3	H	*meta*	0.76 ± 0.03	65.2 ± 4.2	86
19	Z^2	OCH_3	OCH_3	H	*meta*	1.31 ± 0.06	72.0 ± 4.9	55
20	Z^2	H	H	CH_3	*para*	1.76 ± 0.13	79.3 ± 4.8	45

[a] Human recombinant AChE and BuChE from human serum were used. IC_{50} values represent the concentration of inhibitor required to decrease enzyme activity by 50% and are the mean of two independent measurements, each performed in triplicate (SEM = standard error of the mean).

rahedral intermediate interacted with the glycine residues of the oxyanion hole (Figure 2a). In particular, the glycine NH backbone interacted through H bonds with this oxygen atom. The H bond between the protonated nitrogen and the Tyr 124 side chain oxygen was lost, and a new interaction was observed between the protonated nitrogen and the Ser 125 side chain oxygen. The benzene linked to the coumarin ring established quite stable π–π and/or hydrophobic interactions with Trp 286.

The dynamic behavior of the AChE–**9** binary complex is reported in Figure 1b. Compound **9** is the *meta*-coumarin analogue. This was thermally less stable than compound **5** (Figure 1b), highlighting a potentially less stable enzyme–inhibitor complex (Figure 2b). This could explain the weaker inhibition observed against the enzyme. In fact, compound **9** was five- to sevenfold less active than the other compounds investigated by means of docking and MD.

In the AChE–**13** complex, the quaternary anionic moiety of compound **13** interacted with the oxyanion hole formed by the NH backbone of Gly 121 and Gly 122 (Figure 2c). During the MD simulations (Figure 1c), the protonated nitrogen lost the docking identified cation-π interaction with Trp 86 and established a new H bond, which was stable throughout 7 ns of simulation, with the oxygen of the Tyr 124 side chain.

Finally, we analyzed the binary AChE–**16** complex, the most potent compound reported herein. The phenyl ring of compound **16** established a T-shaped stacking interaction with Trp 86 of the central anionic site, which was stable throughout the simulation (Figure 2d). During the MD simulations (Figure 1d), Asp 74 and Tyr 124 got closer to the protonated nitrogen establishing moderately strong electrostatic and H-bonding interaction with compound **16**, respectively. The phenyl ring linked to the chromone moiety was very close to Trp 286 of the PAS pointing to a further π–π stacking interaction between the inhibitor and the enzyme. This interaction was very stable during the MD simulations. Clearly, the seven methylene spacer was the optimal length to allow the phenyl ring linked to the heterocycle to contact Trp 286 of PAS. This was previously pointed to by MD simulations carried out with the crystallographic structure of the Torpedo californica isoform of the enzyme (TcAChE).[16,17]

In brief, some general SAR could be elucidated from the data reported for the pseudo-irreversible AChE inhibitors described. The seven methylene spacer allowed the benzene moiety linked to the heterocycles (coumarins or chromones) to interact with the Trp 286, whereas the heterocycles themselves protruded towards the solvent-exposed gorge entrance. This is known to be an important feature for the inhibition of AChE-induced Aβ aggregation.[17]

Furthermore, unlike previously reported derivatives, where the electronic features of the heterocycle were necessary to anchor the inhibitors in the AChE binding gorge through interaction with Trp 286,[16,26] interaction of the phenyl ring of the inhibitors described herein with the Trp 286 residue did not modulate their inhibitory activity against AChE. Additionally, the methyl group linked to the carbamate moiety allowed the inhibitor to properly fit at the AChE esteratic site, avoiding steric hindrance that could destabilize the quaternary intermediate complex. Remarkably, most of the present modeling results were previously predicted on the basis of simulations carried out with the TcAChE,[16,17] thus validating the newly developed protocol that used both DFT computations and the human isoform of the enzyme.

In light of these computational results, we were prompted to test compounds **5** and **13** (two prototypical *para*-derivatives) and compound **16** (the most active AChE inhibitor of the series) to evaluate their capability to inhibit the AChE-induced Aβ aggregation; these compounds all contain heterocycles that project beyond the PAS. The percent inhibition of AChE-induced Aβ aggregation at 100 μM for compounds **5, 13** and **16** was 12.7 ± 0.1, 17.9 ± 2.0 and 17.2 ± 0.1%, respectively. These compounds are weak inhibitors of AChE-induced Aβ aggregation, with inhibitory activity in the micromolar range. While the inhibitory activities are quite low, these data confirm the hypothesis that both heterocycles can be suitable for the interaction with Trp 286, and in turn for the inhibition of the AChE-induced Aβ aggregation. The inhibitor concentration in

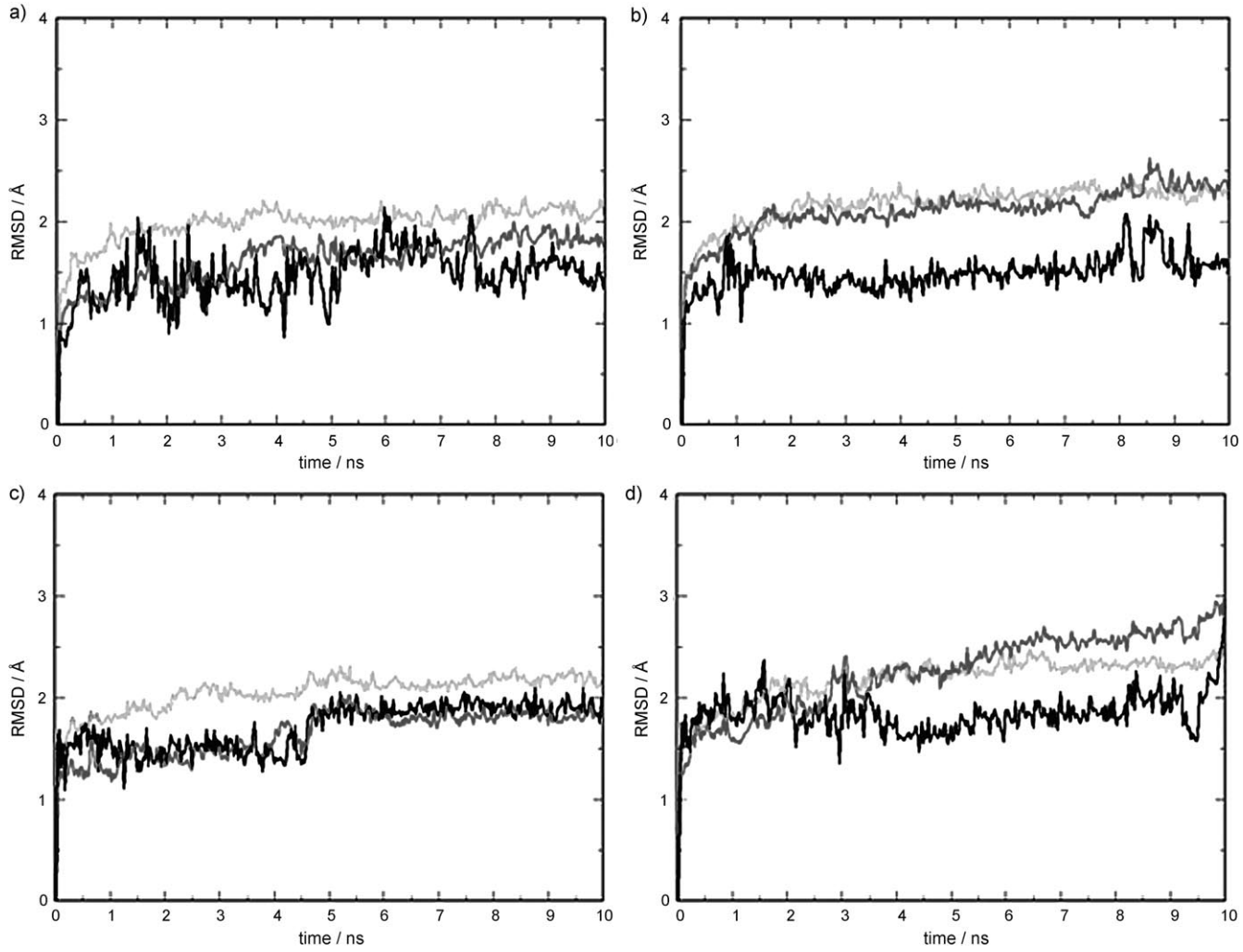

Figure 1. Fluctuations of protein and inhibitor nonhydrogen atoms during MD simulations. Root mean square deviation (RMSD) of the AChE–inhibitor covalent binary complexes plotted as a function of the simulation time. The light grey plot shows the AChE backbone RMSD; the dark grey plot shows the RMSD of residues 7 Å from the ligand; the black plot shows the RMSD of the inhibitor all atoms. a) RMSD of AChE–**5** complex; b) RMSD of AChE–**9** complex; c) RMSD of AChE–**13** complex; d) RMSD of AChE–**16** complex.

the aggregation assay is much higher than the IC_{50} values of the same compounds, however, as noted elsewhere,[27] if these values are normalized on the basis of the different amount of enzyme used in the Ellman's and aggregation assays, the ratio [inhibitor]/[AChE] is of the same order of magnitude in both assays. Consequently, it seems plausible that similar amounts of inhibitor can simultaneously carry out both the anti-cholinesterase and anti-aggregating actions.

Conclusions

In conclusion, we reported a new series of carbamate inhibitors of AChE based on our previous series of inhibitors derived from xantostigmine. The aim of this study was to optimize the methylene chain length for achieving Aβ aggregation inhibition. We clearly showed that, while the parent compound **2** was almost inactive against AChE-induced Aβ aggregation, the new compounds with a benzopyran skeleton, which is longer and more flexible compared to the xanthone moiety, present a promising profile, proving that a full interaction with the residues around the PAS is required for inhibitory activity.

Experimental Section

Chemistry

General Methods: All melting points were determined in open glass capillaries using a Büchi apparatus and are uncorrected. ^{1}H NMR and ^{13}C NMR spectra were recorded in $CDCl_3$ solution on a Varian Gemini 300 spectrometer with TMS as the internal standard. Mass spectra were recorded on a Waters ZQ 4000 apparatus using electrospray (ES) ionization. Silica gel (230–400 mesh, Merck, Germany) was used for purification with flash chromatography. Compound names were obtained using AUTONOM (Beilstein-Institut and Springer, Germany). Elemental analysis was performed using a Perkin–Elmer 2400 CHN Elemental Analyzer.

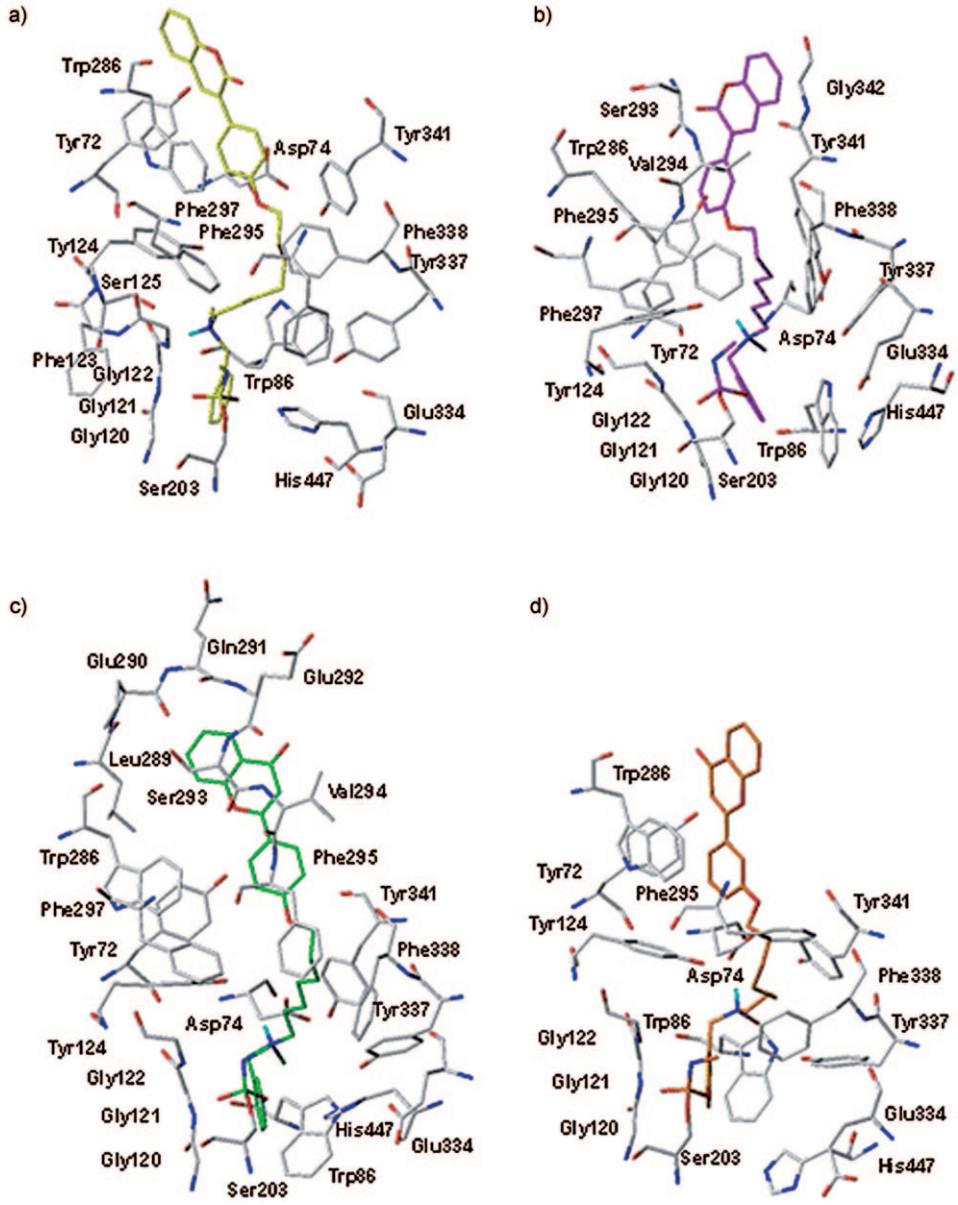

Figure 2. Energy minimized snapshots extracted from equilibrated intervals of the MD simulations and showing AChE–inhibitor binding modes. a) AChE–**5** binary complex (carbon atoms in yellow); b) AChE–**9** binary complex (carbon atoms in magenta); c) AChE–**13** binary complex (carbon atoms in green); d) AChE–**16** binary complex (carbon atoms in orange).

The synthesis of final compounds **3**–**20** was carried out following a standard route (Scheme 1). The synthesis of intermediates **21a** and **22a** are given as an example (below). Full experimental details for all starting materials (schemes S1 and S2) and intermediates **21a-r** and **22a-r** (scheme S3) can be found in the Supporting Information.

3-(7-Bromoheptyloxy)-6-methoxyxanthen-9-one (21a): A stirred suspension of 3-hydroxy-6-methoxyxanthen-9-one[20] (1.21 g, 0.005 mol), 1,7-dibromoheptane (1.7 g, 0.0065 mol) and K_2CO_3 (1.3 g, 0.01 mol) in anhyd acetone was refluxed for 24 h. The reaction was monitored by TLC. The hot reaction mixture was filtered and concentrated. The residue was crystallized from EtOH to give compound **21a** (1.55 g, 80%): mp 148–150 °C; ^{1}H NMR δ 1.45–1.55 (m, 6H), 1.80–1.90 (m, 4H), 3.45 (t, J = 8.2 Hz, 2H), 3.95 (s, 3H), 4.10 (t, J = 6.1 Hz, 2H), 6.85–8.25 ppm (m, 6H, Ar). ^{13}C NMR δ = 26.63, 28.74, 29.35, 30.62, 32.98, 34.12, 56.04, 72.34, 102.64, 102.73, 106.92, 107.00, 118.23, 118.98, 130.43, 130.86, 158.34, 158.76, 162.23, 165.43, 187.03 ppm; MS (ES+) m/z: 420 $[M+H]^+$.

3-{7-[(3-Hydroxybenzyl)methylamino]heptyloxy}-6-methoxyxanthen-9-one (22a): A solution of compound **21a** (2.01 g, 0.005 mol) and *N*-(3-hydroxybenzyl)methylamine (1.37 g, 0.01 mol) in toluene (100 mL) was refluxed for 15 h. After cooling, the reaction mixture was washed with H_2O, dried (Na_2SO_4), filtered and concentrated. Crystallization from toluene gave compound **22a** (0.68 g, 29%): mp 125–127 °C; ^{1}H NMR δ = 1.25–1.58 (m, 8H), 1.75–1.85 (m, 2H), 2.22 (s, 3H), 2.40 (t, J = 8.2 Hz, 2H), 3.45 (s, 2H), 3.85 (s, 3H), 4.01 (t, J = 6.2 Hz, 2H), 6.70–8.25 (m, 10H, Ar). ^{13}C NMR δ = 26.63, 28.04, 29.75, 30.03, 30.62, 38.97, 56.04, 56.12, 62.24, 72.34, 102.64, 102.73, 106.92, 107.00, 114.23, 116.23, 118.23, 118.98, 121.65, 129.65, 130.45, 130.82, 137.74, 157.08, 158.34, 158.76, 162.23, 165.43, 187.03 ppm; MS (ES+) m/z: 485 $[M+H]^+$.

General method for the preparation of carbamates (3–20): A mixture of the selected *N*-methyl-*N*-(3-hydroxybenzyl)aminoheptyloxy derivative (0.001 mol), methyl isocyanate (0.001 mol) and NaH (10 mg) in anhyd toluene was stirred at RT for 24 h, quenched with H_2O and then extracted with CH_2Cl_2 (3×20 mL). The organic layer was washed with H_2O (20 mL), dried (Na_2SO_4), filtered and concentrated. The residue was purified by crystallization (petroleum ether) or by flash-chromatography.

Compound **3**: Solid (81%); mp: 137–139 °C (HCl salt, recrystallized from MeOH/Et_2O); ^{1}H NMR: δ = 1.20–1.60 (m, 8H), 1.75–1.85 (m, 2H), 2.20 (s, 3H), 2.38 (t, J = 4.2 Hz, 2H), 2.88 (d, J = 4.0 Hz, 3H), 3.51 (s, 2H), 3.93 (s, 3H), 4.05 (t, J = 6.2 Hz, 2H), 5.10 (broad, 1H, NH), 6.78–8.35 ppm (m, 10H, Ar); ^{13}C NMR: δ = 26.65, 28.03, 28.36, 29.76, 30.08, 30.13, 38.94, 56.03, 56.12, 61.97, 72.35, 102.43, 102.76, 106.97, 107.01, 118.23, 118.94, 119.98, 121.95, 125.85, 128.65, 130.23, 130.67, 136.78, 152.87, 157.82, 158.35, 158.76, 162.23, 162.38, 165.43, 187.09 ppm; MS (ES+) m/z: 533 $[M+H]^+$; Anal. calcd for $C_{31}H_{37}ClN_2O_6$: C 65.43, H 6.55, N 4.92; found: C 65.44, H 6.54, N 4.93.

Compound **4**: Oil (36%); ^{1}H NMR: δ = 1.25–1.60 (m, 8H), 1.75–1.85 (m, 2H), 2.20 (s, 3H), 2.38 (t, J = 4.1 Hz, 2H), 2.88 (d, J = 4.0 Hz, 3H), 3.42 (s, 2H), 3.93 (s, 3H), 3.96 (s, 3H), 4.05 (t, J = 6.2 Hz, 2H), 5.15 (broad, 1H, NH), 6.70–8.25 ppm (m, 9H, Ar); ^{13}C NMR: δ = 25.86, 27.19, 27.87, 28.88, 29.35, 42.15, 56.41, 57.67, 61.89, 68.58, 70.27, 99.55, 100.49, 105.54, 107.12, 107.34, 107.46, 108.09, 108.46, 113.33, 116.04, 119.38, 123.93, 124.56, 125.87, 127.99, 129.37, 132.97, 146.35, 175.46, 185.94, 196.76, 200.04 ppm; MS (ES+) *m/z*: 563 $[M+H]^+$. Anal. calcd for $C_{32}H_{38}N_2O_7$: C 68.31, H 6.81, N 4.98; found: C 68.30, H 6.82, N 4.97.

Compound **5**: Solid (50%); mp: 142–144°C (HCl salt, recrystallized from MeOH/Et_2O); ^{1}H NMR: δ = 1.30–1.60 (m, 8H), 1.75–1.85 (m, 2H), 2.20 (s, 3H), 2.38 (t, J = 9.0 Hz, 2H), 2.88 (d, J = 4.0 Hz, 3H), 3.50 (s, 2H), 4.00 (t, J = 9.0 Hz, 2H), 4.98 (broad, 1H, NH), 6.95–7.80 ppm (m, 13H, Ar); ^{13}C NMR: δ = 25.92, 27.23, 27.64, 29.08, 29.20, 42.20, 57.41, 61.87, 68.04, 114.42, 116.32, 119.81, 119.98, 121.96, 123.56, 124.36, 125.73, 126.77, 126.89, 127.62, 127.87, 128.87, 128.96, 129.73, 130.90, 138.32, 140.95, 151.02, 153.22, 155.24, 159.69, 160.77 ppm; MS (ES+) *m/z*: 529 $[M+H]^+$. Anal. calcd for $C_{32}H_{37}ClN_2O_5$: C 68.01, H 6.60, N 4.96; found: C 68.03, H 6.61, N 4.95.

Compound **6**: Solid (90%); mp: 72–74°C (free base, recrystallized from ligroin); ^{1}H NMR: δ = 1.30–1.60 (m, 8H), 1.75–1.85 (m, 2H), 2.21 (s, 3H), 2.39 (t, J = 6.2 Hz, 2H), 2.85 (d, J = 4.0 Hz, 3H), 3.51 (s, 2H), 3.85 (s, 3H), 4.00 (t, J = 8.1 Hz, 2H), 5.00 (broad, 1H, NH), 6.80–7.80 ppm (m, 12H, Ar); ^{13}C NMR: δ = 26.32, 26.49, 27.32, 27.67, 28.65, 42.14, 54.47, 57.20, 61.77, 68.16, 99.87, 105.25, 106.13, 106.67, 107.15, 110.87, 111.25, 112.89, 114.29, 120.19, 121.37, 121.65, 124.23, 124.65, 125.54, 128.86, 129.37, 130,65, 139.88, 177.02, 184.43, 185.87, 196.47, 200.13 ppm; MS (ES+) *m/z*: 559 $[M+H]^+$. Anal. calcd for $C_{33}H_{38}N_2O_6$: C 70.95, H 6.86, N 5.01; found: C 70.94, H 6.86, N 5.02.

Compound **7**: Solid (72%); mp: 148–150°C (HCl salt, recrystallized from MeOH/Et_2O); ^{1}H NMR: δ = 1.32–1.62 (m, 8H), 1.75–1.85 (m, 2H), 2.20 (s, 3H), 2.38 (t, J = 6.1 Hz, 2H), 2.88 (d, J = 4.0 Hz, 3H), 3.51 (s, 2H), 3.88 (s, 3H), 4.00 (t, J = 6.1 Hz, 2H), 5.10 (broad, 1H, NH), 6.90–7.80 ppm (m, 12H, Ar); ^{13}C NMR: δ = 25.67, 27.31, 27.47, 28.88, 29.17, 29.76, 41.10, 42.29, 56.90, 57.15, 61.49, 68.25, 68.37, 105.43, 114.38, 115.23, 118.02, 121.87, 124.08, 126.65, 126.86, 127.05, 127.61, 127.82, 128.06, 128.93, 129.15, 132.56, 155.26, 161.91, 198.78, 203.98 ppm; MS (ES+) *m/z*: 559 $[M+H]^+$. Anal. calcd for $C_{33}H_{39}ClN_2O_6$: C 66.60, H 6.61, N 4.71; found: C 66.61, H 6.60, N 4.72.

Compound **8**: Solid (52%); mp: 51–53°C (free base, recrystallized from ligroin); ^{1}H NMR: δ = 1.25–1.55 (m, 8H), 1.75–1.80 (m, 2H), 2.15 (s, 3H), 2.30 (t, J = 6.2 Hz, 2H), 2.80 (d, J = 4.0 Hz, 3H), 3.41 (s, 2H), 3.85 (s, 3H), 3.93 (s, 3H), 3.98 (t, J = 8.2 Hz, 2H), 5.00 (broad, 1H, NH), 6.78–7.65 ppm (m, 11H, Ar); ^{13}C NMR: δ = 26.32, 26.49, 27.32, 27.67, 28.65, 42.14, 54.47, 57.20, 61.77, 68.16, 99.87, 105.25, 106.13, 106.67, 107.15, 110.87, 111.25, 112.89, 114.29, 120.19, 121.37, 121.65, 124.23, 124.65, 125.54, 128.86, 129.37, 130,65, 139.88, 177.02, 184.43, 185.87, 196.47, 200.13 ppm; MS (ES+) *m/z*: 589 $[M+H]^+$. Anal. calcd for $C_{34}H_{40}N_2O_7$: C 69.37, H 6.85, N 4.76; found: C 69.35, H 6.86, N 4.77.

Compound **9**: Solid (24%); mp: 88–89°C (free base, recrystallized from ligroin); ^{1}H NMR: δ = 1.35–1.60 (m, 8H), 1.75–1.85 (m, 2H), 2.20 (s, 3H), 2.40 (t, J = 6.1 Hz, 2H), 2.88 (d, J = 4.0 Hz, 3H), 3.51 (s, 2H), 4.00 (t, J = 8.2 Hz, 2H), 5.00 (broad, 1H, NH), 6.95–7.82 ppm (m, 12H, Ar); ^{13}C NMR: δ = 26.43, 28.12, 28.23, 29.13, 30.02, 30.56, 38.33, 56.23, 62.03, 72.53, 106.67, 111.22, 113.91, 114.19, 118.53, 121.37, 121.49, 126.03, 126.34, 126.92, 127.05, 127.84, 128.10, 128.62, 129.27, 134.84, 136.12, 151.29, 152.13, 157.22, 159.43, 162.23 ppm; MS (ES+) *m/z*: 529 $[M+H]^+$. Anal. calcd for $C_{32}H_{36}N_2O_5$: C 72.70, H 6.86, N 5.30; found: C 72.69, H 6.87, N 5.31.

Compound **10**: Solid (50%); mp: 52–54°C (free base, recrystallized from ligroin); ^{1}H NMR: δ = 1.30–1.60 (m, 8H), 1.75–1.85 (m, 2H), 2.20 (s, 3H), 2.38 (t, J = 6.0 Hz, 2H), 2.88 (d, J = 4.0 Hz, 3H), 3.51 (s, 2H), 3.93 (s, 3H), 4.03 (t, J = 8.2 Hz, 2H), 5.10 (broad, 1H, NH), 6.82–7.80 ppm (m, 12H, Ar); ^{13}C NMR: δ = 26.01, 26.54, 27.22, 27.87, 28.56, 42.20, 55.79, 57.40, 61.87, 68.06, 100.401, 105.65, 106.43, 106.87, 107.85, 110.97, 111.75, 112.79, 114.69, 120.59, 120.87, 121.45, 124.43, 124.35, 125.54, 128.86, 129.37, 140.08, 176.98, 184.43, 185.87, 197.45, 201.23 ppm; MS (ES+) *m/z*: 559 $[M+H]^+$. Anal. calcd for $C_{33}H_{38}N_2O_6$: C 70.95, H 6.86, N 5.01; found: C 70.93, H 6.85, N 5.01.

Compound **11**: Oil (78%); ^{1}H NMR: δ = 1.25–1.60 (m, 8H), 1.75–1.80 (m, 2H), 2.10 (s, 3H), 2.30 (t, J = 6.1 Hz, 2H), 2.80 (d, J = 4.0 Hz, 3H), 3.51 (s, 2H), 3.78 (s, 3H), 3.98 (t, J = 8.1 Hz, 2H), 4.95 (broad, 1H, NH), 6.81–7.68 ppm (m, 12H, Ar); ^{13}C NMR: δ = 26.58, 27.97, 28.27, 29.69, 30.18, 30.56, 38.96, 55.98, 56.34, 61.83, 72.37, 106.92, 110.79, 114.16, 114.26, 119.83, 120.21, 121.87, 125.76, 126.89, 126.93, 127.09, 127.57, 128.65, 129.48, 134.67, 136.67, 151.82, 152.86, 157.75, 158.23, 161.76, 162.34 ppm; MS (ES+) *m/z*: 559 $[M+H]^+$. Anal. calcd for $C_{33}H_{38}N_2O_6$: C 70.95, H 6.86, N 5.01; found: C 70.96, H 6.86, N 5.02.

Compound **12**: Solid (46%); mp: 36–39°C (free base, recrystallized from ligroin); ^{1}H NMR: δ = 1.25–1.50 (m, 8H), 1.75–1.80 (m, 2H), 2.20 (s, 3H), 2.30 (t, J = 6.2 Hz, 2H), 2.80 (d, J = 4.0 Hz, 3H), 3.40 (s, 2H), 3.85 (s, 3H), 3.93 (s, 3H), 4.00 (t, J = 8.2 Hz, 2H), 5.00 (broad, 1H, NH), 6.80–7.70 ppm (m, 11H, Ar); ^{13}C NMR: δ = 26.63, 28.01, 28.32, 29.73, 30.20, 30.63, 38.93, 56.01, 56.34, 56.45, 61.92, 72.35, 106.96, 110.82, 114.11, 114.19, 119.93, 120.12, 121.91, 125.83, 126.52, 126.82, 126.89, 127.63, 128.62, 129.45, 134.63, 136.72, 151.86, 152.83, 157.82, 158.03, 161.63, 162.09 ppm; MS (ES+) *m/z*: 589 $[M+H]^+$. Anal. calcd for $C_{34}H_{40}N_2O_7$: C 69.37, H 6.85, N 4.76; found: C 69.35, H 6.84, N 4.77.

Compound **13**: Solid (77%); mp: 78–80°C (free base, recrystallized from ligroin); ^{1}H NMR: δ = 1.30–1.65 (m, 8H), 1.75–1.85 (m, 2H), 2.20 (s, 3H), 2.39 (t, J = 8.2 Hz, 2H), 2.90 (d, J = 4.0 Hz, 3H), 3.50 (s, 2H), 4.05 (t, J = 6.2 Hz, 2H), 4.98 (broad, 1H, NH), 6.75–8.25 ppm (m, 13H, Ar); ^{13}C NMR: δ = 25.87, 27.11, 27.21, 28.98, 29.07, 29.16, 41.70, 42.09, 57.00, 57.35, 61.79, 68.17, 68.23, 106.00, 114.91, 116.43, 117.92, 120.09, 122.08, 123.65, 123.86, 125.05, 125.61, 125.82, 127.96, 128.93, 129.30, 133.54, 156.16, 162.01, 163.56, 178.45 ppm; MS (ES+) *m/z*: 529 $[M+H]^+$. Anal. calcd for $C_{32}H_{36}N_2O_5$: C 72.70, H 6.86, N 5.30; found: C 72.71, H 6.87, N 5.29.

Compound **14**: Oil (72%); ^{1}H NMR: δ = 1.30–1.65 (m, 8H), 1.75–1.85 (m, 2H), 2.22 (s, 3H), 2.40 (t, J = 8.1 Hz, 2H), 2.86 (d, J = 4.0 Hz, 3H), 3.50 (s, 2H), 3.90 (s, 3H), 4.01 (t, J = 6.0 Hz, 2H), 5.15 (broad, 1H, NH), 6.68–8.19 ppm (m, 12H, Ar); ^{13}C NMR: δ = 25.89, 26.67, 27.16, 27.23, 29.00, 29.17, 29.67, 41.83, 42.12, 55.79, 57.09, 57.39, 61.82, 68.23, 100.36, 105.91, 114.19, 114.60, 114.88, 116.37, 117.72, 120.09, 120.91, 122.09, 123.75, 125.84, 126.97, 127.82, 128.95, 129.31, 157.90, 161.87, 164.04 ppm; MS (ES+) *m/z*: 559 $[M+H]^+$. Anal. calcd for $C_{33}H_{38}N_2O_6$: C 70.95, H 6.86, N 5.01; found: C 70.96, H 6.85, N 5.01.

Compound **15**: Oil (90%); ^{1}H NMR: δ = 1.30–1.63 (m, 8H), 1.75–1.85 (m, 2H), 2.20 (s, 3H), 2.40 (t, J = 4.0 Hz, 2H), 2.87 (d, J = 4.0 Hz, 3H), 3.52 (s, 2H), 3.91 (s, 3H), 4.01 (t, J = 6.1 Hz, 2H), 5.23 (broad, 1H, NH), 6.73–7.88 ppm (m, 12H, Ar); ^{13}C NMR: δ = 26.54, 28.01, 28.36, 29.75, 30.00, 30.69, 38.75, 56.12, 56.15, 61.95, 72.35, 94.91,

114.12, 114.21, 116.07, 118.65, 119.93, 120.25, 121.93, 125.73, 126.50, 126.92, 127.57, 128.59, 129.54, 134.68, 136.75, 151.92, 152.86, 157.79, 158.13, 161.49, 162.12 ppm; MS (ES+) *m/z*: 559 $[M+H]^+$. Anal. calcd for $C_{33}H_{38}N_2O_6$: C 70.95, H 6.86, N 5.01; found: C 70.94, H 6.85, N 5.02.

Compound **16**: Solid (24%); mp: 88–89°C (free base, recrystallized from ligroin); ^{1}H NMR: $\delta = 1.30$–1.63 (m, 8H), 1.78–1.88 (m, 2H), 2.20 (s, 3H), 2.38 (t, $J = 6.2$ Hz, 2H), 2.88 (d, $J = 4.0$ Hz, 3H), 3.48 (s, 2H), 4.05 (t, $J = 6.2$ Hz, 2H), 5.18 (broad, 1H, NH), 6.82–8.25 ppm (m, 13H, Ar); ^{13}C NMR: $\delta = 25.97$, 27.26, 27.68, 29.13, 29.24, 42.16, 57.41, 61.85, 68.25, 107.76, 112.37, 115.34, 116.56, 117.69, 118.11, 118.53, 119.23, 120.09, 121.67, 121.84, 122.06, 122.76, 123.45, 124.13, 124.87, 125.22, 125.68, 125.83, 128.94, 130.08, 133.76, 159.56, 202.38 ppm; MS (ES+) *m/z*: 529 $[M+H]^+$. Anal. calcd for $C_{32}H_{36}N_2O_5$: C 72.70, H 6.86, N 5.30; found: C 72.72, H 6.85, N 5.31.

Compound **17**: Oil (78%); ^{1}H NMR: $\delta = 1.30$–1.65 (m, 8H), 1.75–1.85 (m, 2H), 2.22 (s, 3H), 2.40 (t, $J = 8.1$ Hz, 2H), 2.88 (d, $J = 4.0$ Hz, 3H), 3.50 (s, 2H), 3.98 (s, 3H), 4.05 (t, $J = 6.1$ Hz, 2H), 5.05 (broad, 1H, NH), 6.82–8.20 ppm (m, 12H, Ar); ^{13}C NMR: $\delta = 25.89$, 26.79, 27.21, 29.05, 29.08, 42.01, 55.83, 57.14, 61.93, 68.18, 100.37, 107.48, 112.28, 114.42, 114.59, 116.37, 117.59, 117.67, 118.38, 120.80, 120.91, 122.12, 123.56, 125.33, 126.19, 129.21, 130.03, 132.97, 156.70, 159.49, 163.15, 164.29, 178.14 ppm; MS (ES+) *m/z*: 559 $[M+H]^+$. Anal. calcd for $C_{33}H_{38}N_2O_6$: C 70.95, H 6.86, N 5.01; found: C 70.93, H 6.87, N 5.02.

Compound **18**: Oil (50%); ^{1}H NMR: $\delta = 1.30$–1.65 (m, 8H), 1.75–1.85 (m, 2H), 2.26 (s, 3H), 2.48 (t, $J = 6.1$ Hz, 2H), 2.88 (d, $J = 4.0$ Hz, 3H), 3.59 (s, 2H), 3.93 (s, 3H), 4.05 (t, $J = 6.2$ Hz, 2H), 5.10 (broad, 1H, NH), 6.82–7.60 ppm (m, 12H, Ar); ^{13}C NMR: $\delta = 26.62$, 28.11, 28.42, 29.67, 30.10, 30.72, 38.71, 56.15, 56.18, 62.04, 72.37, 94.98, 113.92, 114.17, 115.97, 118.56, 119.98, 120.18, 121.96, 125.69, 126.53, 126.87, 127.59, 128.51, 129.35, 134.18, 136.55, 151.72, 152.76, 157.59, 158.33, 161.79, 162.25 ppm; MS (ES+) *m/z*: 559 $[M+H]^+$. Anal. calcd for $C_{33}H_{38}N_2O_6$: C 70.95, H 6.86, N 5.01; found: C 70.96, H 6.85, N 5.01.

Compound **19**: Oil (25%); ^{1}H NMR: $\delta = 1.25$–1.60 (m, 8H), 1.75–1.85 (m, 2H), 2.20 (s, 3H), 2.38 (t, $J = 8.1$ Hz, 2H), 2.88 (d, $J = 4.0$ Hz, 3H), 3.49 (s, 2H), 3.93 (s, 3H), 3.95 (s, 3H), 4.00 (t, $J = 6.1$ Hz, 2H), 5.00 (broad, 1H, NH), 6.78–7.58 ppm (m, 11H, Ar); ^{13}C NMR: $\delta =$ 25.17, 27.45, 27.56, 28.48, 29.27, 29.55, 42.13, 42.39, 55.32, 55.75, 62.49, 68.25, 68.87, 104.23, 115.38, 116.33, 118.12, 121.67, 123.18, 126.45, 126.85, 127.15, 127.57, 127.98, 128.16, 128.43, 129.36, 130.35, 131.32, 132.78, 155.09, 161.41, 199.76, 202.18 ppm; MS (ES+) *m/z*: 589 $[M+H]^+$. Anal. calcd for $C_{34}H_{40}N_2O_7$: C 69.37, H 6.85, N 4.76; found: C 69.38, H 6.85, N 4.75.

Compound **20**: Oil (50%); ^{1}H NMR: $\delta = 1.35$–1.65 (m, 8H), 1.75–1.85 (m, 2H), 2.18 (s, 3H), 2.20 (s, 3H), 2.40 (t, $J = 8.9$ Hz, 2H), 2.88 (d, $J = 4.0$ Hz, 3H), 3.51 (s, 2H), 3.93 (s, 3H), 4.05 (t, $J = 6.2$ Hz, 2H), 5.10 (broad, 1H, NH), 6.78–8.15 ppm (m, 12H, Ar); ^{13}C NMR: $\delta =$ 24.87, 26.46, 26.89, 27.38, 29.17, 29.47, 42.32, 42.78, 54.22, 55.85, 61.89, 67.72, 68.95, 103.63, 114.27, 116.23, 118.82, 121.79, 123.08, 125.45, 126.75, 127.25, 127.37, 128.04, 128.26, 128.73, 129.16, 130.95, 131.32, 132.78, 199.76, 202.18 ppm; MS (ES+) *m/z*: 543 $[M+H]^+$. Anal. calcd for $C_{33}H_{38}N_2O_5$: C 73.04, H 7.06, N 5.16; found: C 73.05, H 7.06, N 5.15.

Biology

Inhibition of AChE and BuChE

The method of Ellman et al. was followed.[21] Five different concentrations of each compound were tested to obtain 20–80% inhibition of AChE or BuChE. The assay solution consisted of a potassium phosphate buffer (0.1 M, pH 8.0), with 5,5′-dithio-bis(2-nitrobenzoic acid) (340 μM), human recombinant AChE or BuChE (0.02 U mL^{-1}) derived from human serum (Sigma Chemical), and substrate (acetylthiocholine iodide or butyrylthiocholine iodide, 550 μM). Test compounds were added to the assay solution and preincubated with the enzyme for 20 min at 37°C followed by addition of substrate. Assays were carried out with a blank containing all components except AChE or BuChE in order to measure nonenzymatic reactions. The reaction rates were compared, and the percent inhibition due to the presence of test compounds was calculated. Each concentration was analyzed in triplicate, and IC_{50} values were determined graphically from inhibition curves (log[inhibitor] vs percent inhibition).

Inhibition of AChE-induced β-amyloid aggregation

Aliquots of 2 μL Aβ(1-40) peptide (Bachem AG, Germany), lyophilized from a HFIP (1,1,1,3,3,3-hexafluoro-2-propanol) solution (2 mg mL^{-1}) and dissolved in DMSO, were incubated for 24 h at room temperature in sodium phosphate buffer (0.215 M, pH 8.0) at a final concentration of 230 μM. For co-incubation experiments, aliquots (16 μL) of human recombinant AChE (final concentration 2.30 μM, Aβ/AChE molar ratio 100:1) and AChE in the presence of test inhibitor (2 μL, 100 μM final concentration) were added. Blanks containing Aβ, AChE, and Aβ plus inhibitors, in sodium phosphate buffer (0.215 M, pH 8.0) were prepared. The final volume of each vial was 20 μL. Each assay was run in duplicate.

To quantify amyloid fibril formation, the thioflavin T fluorescence method was then applied.[27–29] Analyses were performed with a Jasco Spectrofluorometer FP-6200 using a 3 mL quartz cell. After incubation, the samples containing Aβ, Aβ+AChE, or Aβ+AChE+inhibitors were diluted with glycine–NaOH buffer (50 mM, pH 8.5) containing thioflavin T (1.5 μM) to a final volume of 2.0 mL. A 300 s time scan of the emitted fluorescence ($\lambda_{exc} = 446$ nm, $\lambda_{em} =$ 490 nm) was performed and the intensity values at the plateau were averaged after subtracting the background fluorescence of thioflavin T (1.5 μM) and AChE.

The fluorescence intensities in the presence and absence of inhibitor were compared and the percentage of inhibition was calculated: $100\text{-}(IF_i/IF_o \times 100)$ where IF_i and IF_o are the fluorescence intensities obtained for Aβ+AChE in the presence and absence of inhibitor, respectively.[27]

Docking and molecular dynamics simulations

The 3D models of compounds **13**, **16**, **5**, and **9** were built using Sybyl 7.1.1 (Tripos Associates Inc, USA) and geometry optimized at density functional level of theory (B3LYP/6-31G*) by means of the software Gaussian 03.[30] Docking simulations were carried out by means of the AutoDock software 3.0[22] using the hAChE–fasciculin co-crystal structure (PDB code 1B41).[23] Fasciculin was removed and the ligand binding site was defined as 10 Å from the oxygen of the Tyr 124 side chain. Standard AutoDock runs were unable to generate a docking pose between the inhibitors and the enzyme that resembled the Michaelis complex. In light of this, new Auto-

Dock parameters were defined for the oxygen of the Ser203 side chain and the carbamate carbon of the inhibitors (i.e., the atoms involved in the formation of the covalent bond in the tetrahedral intermediate). In particular, the new parameters forced the inhibitor to get close (1.20 Å) to Ser203 for the subsequent formation of the covalent bond between the two atoms. In this way, docking poses resembling the Michaelis complexes were generated, and one low energy conformation was selected for DFT-based optimization and parameterization. The covalent bond between the inhibitor and the enzyme was drawn manually and a model system of 34 atoms was submitted to DFT calculations at B3LYP/6-31G* and geometrically optimized reaching the standard G03 criterion of convergence on the gradient (see Supporting Information). The DFT optimized intermediate was docked at the AChE esteratic site replacing the same moiety of the unbound inhibitor. The same procedure was applied to compounds **13**, **16**, **5**, and **9**. RESP charges[31] were calculated capping Ser203 with ACE and NME at the N and C termini, respectively. Generalized Amber Force Field (GAFF) was used for nonstandard parameters, keeping the default parameter close to the output of DFT/B3LYP/6-31G* geometry.

The binary complexes between AChE and compounds **13**, **16**, **5**, and **9** were investigated by means of MD simulations carried out with the AMBER 8.0 software. MD simulations (10 ns) on the binary complexes were carried out in explicit solvent and periodic boundary conditions. Six Na^+ counterions were added to the solvent bulk of the protein–water complexes to maintain neutrality in the systems. First, water shells and counterions were minimized using steepest descent and conjugate gradient algorithms. Then, a minimization of the entire complex was performed setting a convergence criterion with a gradient of 0.001 kcal mol^{-1} $Å^{-1}$. Equilibration runs were carried out by heating the system to 300 K in 100 ps. This was followed by MD simulations (7 ns) in the NPT ensemble (constant temperature and pressure). The parm99 version[32] of the all atom Amber force field[33] was used for the protein and the counterions, whereas the TIP3P model[34] was employed to explicitly represent water molecules. The van der Waals and short range electrostatic interactions were estimated within a 10 Å cutoff, whereas the long range electrostatic interactions were assessed by using the particle mesh Ewald (PME) method,[35] with ~1 Å charge grid spacing interpolated by fourth order B-spline, and by setting the direct sum tolerance to 10^{-5}. Bonds involving hydrogen atoms were constrained by using the SHAKE algorithm[36] with a relative geometric tolerance for coordinate resetting of 0.00001 Å. Berendsen's coupling algorithms[37] were employed to maintain constant temperature and pressure with the same scaling factor for both solvent and solutes, and with the time constant for heat bath coupling maintained at 1.5 ps. The pressure for the isothermal-isobaric ensemble was regulated by using a pressure relaxation time of 1 ps in the Berendsen's algorithm. The simulations of the solvated protein models were performed using constant pressures of 1 atm and constant temperature of 300 K. All calculations were performed on a Linux cluster employing an openMosix architecture.

Acknowledgements

This work was supported by MIUR, (FIRB RBNE03FH5Y), Rome (Italy).

Keywords: drug design · neurological agents · Alzheimer's disease · flavones · coumarins

[1] A. Alzheimer, *Allg. Z. Psychiatr.* **1907**, 146–148.
[2] D. J. Selkoe, *Ann. Intern. Med.* **2004**, *140*, 627–638.
[3] S. Love, *J. Neurol. Neurosurg. Psychiatry* **2005**, *76(S5)*, 8–14.
[4] L. Buée, T. Bussière, V. Buée-Scherrer, A. Delacourte, P. R. Hof, *Brain Res. Rev.* **2000**, *33*, 95–130.
[5] E. Giacobini, *Int. J. Geriatr. Psychiatry* **2003**, *18*, S1-S5.
[6] I. Silman, J. L. Sussmann, *Curr. Opin. Pharmacol.* **2005**, *5*, 293–302.
[7] A. V. Terry, J. J. Buccafusco, *J. Pharmacol. Exp. Ther.* **2003**, *306*, 821–827.
[8] P. Valenti, A. Rampa, A. Bisi, G. Fabbri, V. Andrisano, V. Cavrini, *Med. Chem. Res.* **1995**, *5*, 255–264.
[9] A. Rampa, A. Bisi, P. Valenti, M. Recanatini, A. Cavalli, V. Andrisano, V. Cavrini, L. Fin, A. Buriani, P. Giusti, *J. Med. Chem.* **1998**, *41*, 3976–3986.
[10] M. Harel, I. Schalk, L. Ehret-Sabatier, F. Bouet, M. Goeldner, C. Hirth, P. H. Axelsen, I. Silman, J. L. Sussman, *Proc. Natl. Acad. Sci. USA* **1993**, *90*, 9031–9035.
[11] Y. Bourne, P. Taylor, Z. Radić, P. Marchot, *EMBO J.* **2003**, *22*, 1–12.
[12] A. Cavalli, G. Bottegoni, C. Raco, M. De Vivo, M. Recanatini, *J. Med. Chem.* **2004**, *47*, 3991–3999.
[13] N. C. Inestrosa, A. Alvarez, C. A. Pérez, R. D. Moreno, M. Vicente, C. Linker, O. I. Casanueva, C. Soto, J. Garrido, *Neuron* **1996**, *16*, 881–891.
[14] M. Recanatini, P. Valenti, *Curr. Pharm. Des.* **2004**, *10*, 3157–3166.
[15] G. V. De Ferrari, M. A. Canales, I. Shin, L. M. Weiner, I. Silman, N. C. Inestrosa, *Biochemistry* **2001**, *40*, 10447–10457.
[16] A. Rampa, L. Piazzi, F. Belluti, S. Gobbi, A. Bisi, M. Bartolini, V. Andrisano, V. Cavrini, A. Cavalli, M. Recanatini, P. Valenti, *J. Med. Chem.* **2001**, *44*, 3810–3820.
[17] F. Belluti, A. Rampa, L. Piazzi, A. Bisi, S. Gobbi, M. Bartolini, V. Andrisano, A. Cavalli, M. Recanatini, P. Valenti, *J. Med. Chem.* **2005**, *48*, 4444–4456.
[18] H. Sugimoto, Y. Yamanishi, Y. Iimura, Y. Kawakami, *Curr. Med. Chem.* **2000**, *7*, 303–339.
[19] L. Piazzi, A. Rampa, A. Bisi, S. Gobbi, F. Belluti, A. Cavalli, M. Bartolini, V. Andrisano, P. Valenti, M. Recanatini, *J. Med. Chem.* **2003**, *46*, 2279–2282.
[20] L. Piazzi, F. Belluti, A. Bisi, S. Gobbi, S. Rizzo, M. Bartolini, V. Andrisano, M. Recanatini, A. Rampa, *Bioorg. Med. Chem.* **2007**, *15*, 575–585.
[21] G. L. Ellman, K. D. Courtney, V. Andres, R. M. Featherstone, *Biochem. Pharmacol.* **1961**, *7*, 88–95.
[22] G. M. Morris, D. S. Goodsell, R. S. Halliday, R. Huey, W. E. Hart, R. K. Belew, A. J. Olson, *J. Comput. Chem.* **1998**, *19*, 1639–1662.
[23] G. Kryger, M. Harel, K. Giles, L. Toker, B. Velan, A. Lazar, C. Kronman, D. Barak, N. Ariel, A. Shafferman, I. Silman, J. L. Sussman, *Acta Crystallogr. Sect. D: Biol. Crystallogr.* **2000**, *56*, 1385–1394.
[24] C. Bartolucci, E. Perola, L. Cellai, M. Brufani, D. Lamba, *Biochemistry* **1999**, *38*, 5714–5719.
[25] D. A. Case, T. E. Darden, T. E. I. Cheatham, C. L. Simmerling, J. Wang, R. E. Duke, R. Luo, K. M. Merz, B. Wang, D. A. Pearlman, M. Crowley, S. Brozell, V. Tsui, H. Gohlke, J. Mongan, V. Hornak, G. Cui, P. Beroza, C. Schafmeister, J. W. Caldwell, W. S. Ross, P. A. Kollman, *AMBER 8*; University of California: San Francisco.
[26] L. Piazzi, A. Cavalli, F. Belluti, A. Bisi, S. Gobbi, S. Rizzo, M. Bartolini, V. Andrisano, M. Recanatini, A. Rampa, *J. Med. Chem.* **2007**, *50*, 4250–4254.
[27] M. Bartolini, C. Bertucci, V. Cavrini, V. Andrisano, *Biochem. Pharmacol.* **2003**, *65*, 407–416.
[28] H. Naiki, K. Higuchi, K. Nakakuki, T. Takeda, *Lab. Invest.* **1991**, *65*, 104–110.
[29] H. LeVine, *Protein Sci.* **1993**, *2*, 404–410.
[30] M. J. Frisch, G. W. Trucks, H. B. Schlegel, G. E. Scuseria, M. A. Robb, J. R. Cheeseman, V. G. Zakrzewski, J. A., Jr., Montgomery, R. E. Stratmann, J. C. Burant, S. Dapprich, J. M. Millam, A. D. Daniels, K. N. Kudin, M. C. Strain, O. Farkas, J. Tomasi, V. Barone, M. Cossi, R. Cammi, B. Mennucci, C. Pomelli, C. Adamo, S. Clifford, J. Ochterski, G. A. Petersson, P. Y. Ayala, Q. Cui, K. Morokuma, D. K. Malick, A. D. Rabuck, K. Raghavachari, J. B. Foresman, J. Cioslowski, J. V. Ortiz, B. B. Stefanov, G. Liu, A. Liashenko, P. Piskorz, I. Komaromi, R. Gomperts, R. L. Martin, D. J. Fox, T. Keith, M. A. Al-Laham, C. Y. Peng, A. Nanayakkara, C. Gonzalez, M. Challacombe, P. M. W. Gill, B. G. Johnson, W. Chen, M. W. Wong, J. L. Andres, M. Head-Gordon, E. S. Replogle, J. A. Pople, *Gaussian 03 Revision C.02*; Gaussian, Inc.: Pittsburgh, PA.
[31] C. I. Bayly, P. Cieplak, W. D. Cornell, P. A. Kollman, *J Phys Chem.* **1993**, *97*, 10269.
[32] J. Wang, P. Cieplak, P. A. Kollman, *J. Comput. Chem.* **2000**, *21*, 1049–1074.

[33] W. D. Cornell, P. Cieplak, C. I. Bayly, I. R. Gould, K. M. Merz, D. M. Ferguson, D. C. Spellmeyer, T. Fox, J. W. Caldwell, P. A. Kollman, *J. Am. Chem. Soc.* **1995**, *117*, 5179–5197.
[34] W. L. Jorgensen, J. Chandrasekhar, J. D. Madura, R. W. Impey, L. M. Klein, *J. Chem. Phys.* **1983**, *79*, 926–935.
[35] U. Essmann, L. Perera, M. L. Berkowitz, T. Darden, H. Lee, L. G. Pedersen, *J. Chem. Phys.* **1995**, *103*, 8577–8593.
[36] J. P. Ryckaert, G. Ciccotti, H. J. C. Berendsen, *J. Comput. Phys.* **1977**, *23*, 327–341.
[37] H. J. C. Berendsen, J. P. M. Postma, W. F. Van Gunsteren, A. Di Nola, J. R. Haak, *J. Chem. Phys.* **1984**, *81*, 3684–3690.

Received: November 19, 2008
Revised: December 19, 2008
Published online on February 16, 2009

